Necking Instability during Polydomain−Monodomain Transition in a Smectic Main-Chain Elastomer

Harshad P. Patil, Daniel M. Lentz, and Ronald C. Hedden*

Department of Materials Science and Engineering, The Pennsylvania State University, University Park, Pennsylvania 16802

Received January 20, 2009; Revised Manuscript Received March 1, 2009

ABSTRACT: The mechanical response and the evolution of director orientation are characterized in a smectic, main-chain liquid crystalline elastomer (LCE) as it undergoes the familiar polydomain−monodomain (P−M) transition. Under uniaxial tension, the LCE behaves like an ordinary rubber-like network at low strains, and local director rotations are shown to slightly favor the perpendicular ("anomalous") orientation of chain axes with respect to the draw direction. As strain increases, a well-defined yield stress is observed due to the onset of a necking instability. Macroscopic elongation proceeds by growth of the necked monodomain region, which appears to consume the non-necked polydomain region(s) at its boundaries. Within the necked region, the parallel ("normal") orientation of chain axes with respect to the draw direction is strongly favored. The P−M transition is attributed to a change in the conformation of the elastic polymer backbones from hairpinned coils to extended chains. Under the conditions of temperature and strain rate studied, buckling of the smectic layers is observed as the fully necked monodomain state is approached.

1. Introduction

Liquid crystalline elastomers (LCEs) are rubber-like polymer networks that exhibit one or more stable mesophases characterized by orientational and/or limited positional ordering. Among the numerous types of LCEs, smectic elastomers with main-chain mesogenic units arguably exhibit the strongest deviations from ordinary rubber elasticity due to the conformational constraints imposed on the polymer backbone by strong, segment-level positional correlations. As their exceptional mechanical behavior distinguishes smectic main-chain LCEs from all other elastomers, recent efforts have focused on controlling the molecular factors governing the static and dynamic mechanical response[1−3] or on advancing basic understanding of smectic rubber elasticity.[4−6]

Cross-linking a smectic polymer in the absence of an external aligning field produces a polydomain elastomer containing numerous randomly oriented microdomains. The polydomain morphology is stabilized by anchoring of the network chains to fixed cross-link junctions, which are randomly distributed throughout the network. Under uniaxial tension, polydomain LCEs of both nematic and smectic types undergo a well-known transition to a globally oriented "monodomain" state, hereafter referred to as the P−M transition. A mechanical signature of the P−M transition is a plateau in the nominal stress versus strain curve, corresponding to a significant softening of the material. (The nominal stress is defined as σ_n = applied force/original cross-sectional area). In some cases, once a threshold strain is reached, the elastomer may appear to elongate significantly at essentially constant load. A well-defined plateau stress is noted in both nematic and smectic LCEs, including those of both the main-chain[3,7,8] and the side-chain[9−15] types, although the plateau is usually more pronounced in the main-chain elastomers due to higher backbone anisotropy. Zentel et al. also observed softening during uniaxial stretching of a smectic main-chain elastomer that had been cross-linked in the monodomain state,[6] noting that the plateau became less pronounced as the smectic−isotropic clearing temperature was approached.

* To whom correspondence should be addressed. Tel.: (814) 863-2325. Fax: (814) 865-2917. E-mail: hedden@matse.psu.edu.

Despite similarities in the mechanical response during uniaxial elongation, the mechanism for the transition to the globally oriented state at the molecular level is not necessarily universal among the different types of LCE. For instance, the molecular basis for the observed plateau stress may reasonably be expected to differ between main-chain and side-chain LCEs, or between nematic and smectic LCEs. Numerous experimental and theoretical studies have therefore attempted to explain the mechanism of the P−M transition in terms of domain-level director rotations and/or changes in elastic chain conformation occurring in different classes of LCE.

Terentjev et al. developed a theoretical framework for the P−M transition in nematic LCE, under the assumption that the observed plateau stress is due to local director rotations, without growth or destruction of domains.[13,16−18] Director fluctuations become localized within the domain walls as the sample deforms to achieve global alignment.[13] The "soft" modes of deformation that permit local director rotations contribute to the plateau stress observed in nematic LCE.[13,19,20] The plateau stress is predicted by the model without considering any means of elongation at the molecular level except for the local rotation of anisotropically shaped domains.

The plateau stress observed in smectic LCE is less easily explained, however, as energetic penalties are associated with some or all types of director rotations,[4,5] due to the presence of segment-level layering. In a study of smectic main-chain LCE having unusually large domains that could be imaged by polarized optical microscopy, Ortiz et al. observed domain rotations and sharpening of domain boundaries, consistent with theoretical predictions,[7] although elongation of domains in the direction of elongation was also noted. Later, Ortiz et al. argued that stress relaxation in a uniaxially elongated smectic main-chain LCE may proceed through transient breakdown or disordering of smectic layering, followed by redevelopment of smectic order in the globally oriented state.[8]

Recently, Watanabe et al. attributed the P−M transition in smectic C_A main-chain elastomers to a transition in the elastic backbone conformation from hairpinned to extended.[3] Long polymer chains in both smectic LCP and LCE are expected to form hairpins, or simple chain folds, which increase conformational entropy as compared to the extended chain state.

10.1021/ma9001325 CCC: $40.75
Published on Web 04/15/2009

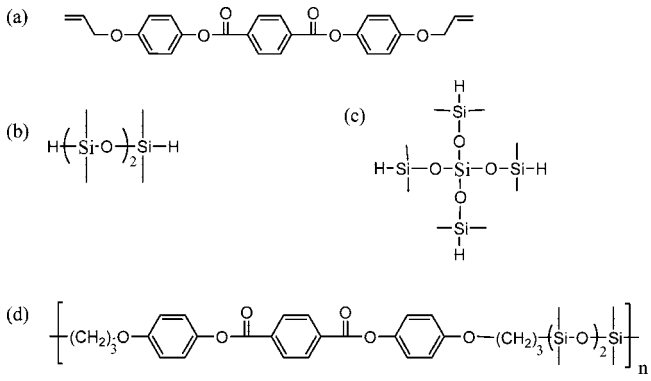

Figure 1. Chemical structures of monomers and polymers: (a) B_2 mesogen; (b) A_2 flexible spacer; (c) A_4 cross-linker; and (d) repeat unit of elastic chains.

Experimental evidence for chain folding in main-chain smectics is found in the "anomalous" layer orientation sometimes observed in smectic LCP subjected to elongation.[2,21,22] The role of hairpin formation in the elasticity of main-chain LCE has recently been discussed theoretically by Adams and Warner,[23] who showed that elongation of hairpinned chains can account for the plateau in the nominal stress associated with the P−M transition.

Previous studies of the P−M transition typically focused on morphological changes occurring at the molecular or domain level to explain the observed mechanical response during uniaxial elongation. However, a complete picture of the uniaxial elongation process must consider the evolution of orientation throughout the entire sample, as inhomogeneous deformation during the P−M transition is possible in at least some LCEs. It is normally reported that an opaque or turbid polydomain sample becomes translucent or nearly transparent during the course of the P−M transition,[6,7,14] but the possibility of strongly nonaffine deformation at a macroscopic level has generally received insufficient attention.

In this Article, we provide some new insights regarding the P−M transition in smectic main-chain elastomers, which lend themselves readily to X-ray studies of molecular orientation due to a bright, low-angle reflection associated with smectic layering. We examine a single smectic polydomain LCE, which undergoes severely nonaffine deformation upon uniaxial elongation. As elongation proceeds, the elastomer develops a distinct "necking" instability, a local contraction that propagates and eventually consumes the entire sample as elongation proceeds. The changes in molecular orientation associated with the necking instability are characterized by polarized optical microscopy and wide-angle X-ray diffraction (WAXD). We discuss changes in elastic chain conformation and director orientation occurring throughout the P−M transition. The relative contributions of local director rotations versus unfolding of hairpinned elastic chains to macroscopic elongation are debated. Finally, we consider the mechanism of elongation at high strains, where most elastic chains are already in highly extended conformations.

2. Experimental Section

2.1. Elastomer Synthesis. The backbone of the LCE studied here had the repeat unit illustrated in Figure 1, with alternating mesogens and flexible oligosiloxane spacers. The LCE was prepared by nonlinear polymerization of mesogen (B_2), spacer (A_2), and cross-linker (A_4) by Pt^0-catalyzed hydrosilylation, similar to a route described by Finkelmann et al.[24] Details of the synthesis of the allyloxy-terminated mesogens (B_2) are presented in a previous report.[2] The reaction was started by mixing A_2, B_2, and A_4 in toluene (50 mass % monomers in toluene) at 80 °C. The hydrosilylation reaction was catalyzed by adding Pt^0-1,3-divinyl-1,1,3,3-tetramethyldisiloxane complex (Alfa Aesar) at a concentration of 1.0 mass % of the total mass of combined monomers (excluding toluene). After 14 days of cure, the toluene was allowed to evaporate by air drying. Postcuring proceeded in air at 80 °C for an additional 1 day, then under vacuum for 1 day. The mole fraction of A groups (SiH) belonging to cross-linkers is defined as

$$\rho \equiv \frac{(\text{moles A groups belonging to branched monomers})}{(\text{total moles A groups})}$$

$$= \frac{4(\text{moles } A_4)}{2(\text{moles } A_2) + 4(\text{moles } A_4)} \quad (1)$$

and ρ was set to 0.06 ± 0.006. The mole ratio of total A groups (SiH) to B groups (allyloxy), or "*r*", was calculated as

$$r = [4(\text{moles } A_4) + 2(\text{moles } A_2)]/[2(\text{moles } B_2)] \quad (2)$$

and r was chosen as 1.3 ± 0.1. We previously examined the significance of varying r and ρ in LCE based upon similar methyl-substituted mesogens.[1] Following cross-linking, the LCE was swollen and extracted in excess toluene for 7 days to remove solubles, during which time the toluene was replaced with fresh solvent daily. The LCE was deswollen by slow addition of methanol (a poor solvent) to the toluene over a period of a few days, to avoid cracking from rapid evaporation of solvent, followed by air drying and vacuum drying at 50 °C.

2.2. Dynamic Mechanical Analysis (DMA). Stress−strain behavior was characterized in uniaxial elongation using a TA Instruments Q800 DMA. Standard dogbone-shaped samples were prepared, having initial length of 7 mm, width of 1.15 mm, and thickness of approximately 0.4 mm. Prior to mechanical testing, samples were subjected to a thermal pretreatment that was found to produce a repeatable mechanical response. Samples were heated to 100 °C for 5 min, then cooled quickly to room temperature and allowed to equilibrate overnight before mechanical testing. Stress−strain curves were obtained at 35 °C by preheating the sample for 15 min., then applying a force ramp at rate of 0.05 N/min until an overall draw ratio of λ was reached, where $\lambda = (L/L_0)$ is calculated from L and L_0, the final and initial sample lengths between the clamps, respectively. Alternatively, stress−strain curves were generated by applying a strain ramp of 12.5%/min, based upon the original sample length, until the desired draw ratio was reached. Tensile tests are identified in the text as either "force ramp" or "strain ramp", respectively.

For preparation of drawn elastomers by WAXD or optical microscopy, samples were elongated to λ at a controlled strain rate of 12.5%/min using the DMA, then allowed to relax for 60 min or more at constant λ. After relaxation, the elastomer was cooled below the glass transition temperature ($T_g \approx 10$ °C) under tension. The rigid elastomer could be removed from the DMA in the glassy state and transferred to a portable stainless steel clamping device that was custom-fabricated to allow mounting in the X-ray diffractometer or the optical microscope. Elastomers were allowed to warm to room temperature before initiating WAXD or microscopy measurements. The local or mesoscopic draw ratio (λ_m) was measured at the location of the incident X-ray beam immediately after the WAXD measurement, using the "ink dot" technique described in section 2.4.

2.3. Wide-Angle X-ray Diffraction (WAXD). Wide-angle X-ray diffraction (WAXD) experiments were performed on samples of 0.4 mm initial thickness at an ambient temperature of 25 ± 2 °C in transmission using a Rigaku D/MAX Rapid II instrument equipped with graphite monochromator, 300 μm pinhole collimator, and Cu Kα source (wavelength = 1.5418 Å). Corrections for polarization and oblique incidence were applied to raw data using Rigaku AreaMax software. Samples were subjected to a specified overall uniaxial elongation of magnitude λ at a controlled strain rate at 35 °C using the DMA, and transferred to the portable clamping device as described in section 2.2. Samples were mounted in the X-ray diffractometer such that the incident X-ray beam was

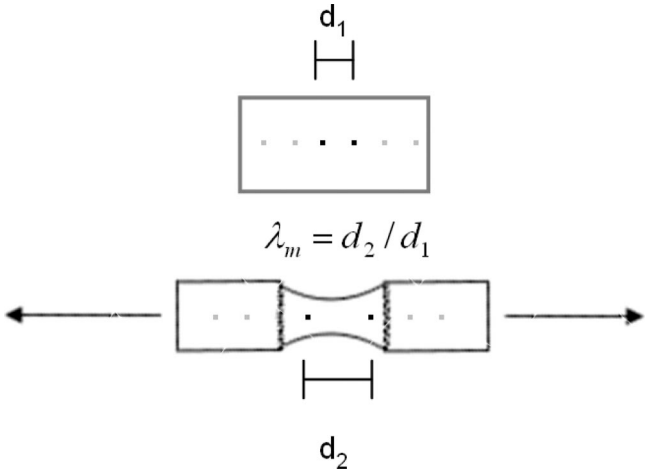

Figure 2. Illustration of "ink dot" technique for determining the mesoscopic draw ratio (λ_m) for an inhomogeneously deformed elastomer in the necked state.

normal to the axis of elongation. The incident X-ray beam generally passed through the thinnest portion of the sample far from the clamps, except where otherwise indicated. Sufficient time was allowed for the sample to come to ambient temperature of 25 °C before WAXD data were collected.

After subtraction of background scattering, the low-angle reflection centered at $2\theta \approx 2.9°$ was integrated over the range $2.0° < 2\theta < 3.8°$ to obtain $I(\chi)$, where χ is the azimuthal angle. The axis of elongation, hereafter denoted as z, was set to coincide with $\chi = 0°$ and 180°.

2.4. Polarized Optical Microscopy (POM). Samples were characterized via orthoscopic observation between crossed polarizers in an Olympus BX51 microscope with UMPlanFL 1.25× or 5× objectives. Samples were elongated at a controlled strain rate using the DMA and transferred to the microscope as described in section 2.2. Alternatively, samples could be elongated using a screw-driven, manually operated stretching device, to observe the P−M transition in situ. Images were recorded using a 2.0 megapixel Diagnostic Instruments model # 11.2 Color Mosaic digital camera equipped with Spot digital imaging software.

Both λ and λ_m were determined photographically in the microscope by an "ink dot" technique (Figure 2). A line of approximately 5−15 black dots was applied to the elastomer surface using a water-based ink that was not measurably absorbed by the elastomer (Speedball 3400-Black water-soluble block printing ink). The positions of the dots were recorded photographically through the microscope in the unstretched condition, then again after stretching. The overall draw ratio (λ) was determined by comparing the separation between the clamps before and after stretching. Values of λ_m were found by comparison of adjacent ink dots before and after stretching. Separate values of λ_m could thus be found for the necked and non-necked portions of the sample for inhomogeneous deformations. Similarly, λ_m could be measured in the exact location where the X-ray beam was directed for WAXD measurements. Alternatively, the ink dots could be applied to the elastomer in the stretched condition, after WAXD or optical microscopy experiments were completed. The elastomer was then returned to the undeformed polydomain state by heating to 100 °C for 5 min, allowing isotropization and relaxation, followed by cooling to ambient temperature, after which the separation between dots was measured again. The elastomer returned repeatedly to its original shape and dimensions even after several deformation cycles.

3. Results and Discussion

3.1. Thermal Behavior. The elastomer studied here is similar to one described by us in a previous communication (E−H) except for some minor differences in the curing conditions.[2] These elastomers exhibit a single smectic phase between the glass transition temperature (approximately 10 °C) and the clearing temperature. The smectic−isotropic clearing transition occurs over a broad temperature range between about 70 and 110 °C, judging by the maximum in the mechanical loss tangent observed in small-strain oscillatory shear.[2] A non-cross-linked, linear polymer of the same backbone structure had a clearing temperature of approximately 130 °C and exhibited a S_{CA} mesophase between 52 °C < T < 130 °C.[2] The linear polymer undergoes a transition to a higher order smectic state below 52 °C, but no X-ray or thermal evidence for this transition was found in the elastomer. All mechanical tests described herein were conducted at 35 °C, well below the smectic−isotropic clearing temperature. No evidence for crystallization was found by X-ray diffraction for the elastomer at any temperature or after stretching.

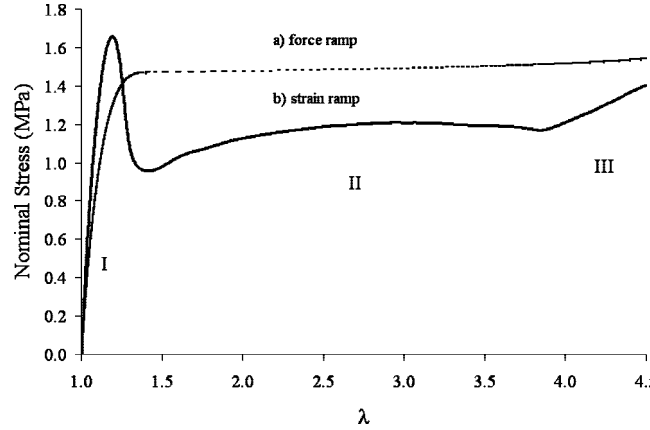

Figure 3. Plot of nominal stress versus strain for smectic main-chain LCE: (a) as observed by applying a force ramp; (b) as observed by applying a strain ramp. Details of mechanical tests are described in the Experimental Section.

3.2. Uniaxial Elongations. Several dogbone-shaped samples were punched from a single sheet of the extracted elastomer and were subjected to uniaxial elongation by different protocols. A "force ramp" tensile test was conducted by increasing the tensile load linearly at a rate of 0.05 N/min, corresponding to an increase in the nominal stress at a rate of approximately 0.11 MPa/min. Although the nominal stress increases linearly with time in this method, the true stress increases at a nonlinear rate as the cross-sectional area of the sample decreases. A "strain ramp" tensile test was also conducted by increasing the overall strain linearly at a rate of 12.5%/min, based upon the initial length of the sample. Figure 3 compares the dependence of nominal stress (σ_n) on the macroscopic draw ratio ($\lambda \equiv L/L_0$) for both tensile tests. Stress−strain curves are divided into three regions, hereafter denoted I, II, and III for consistency with earlier studies.[8,14]

Region I is characterized by a steep increase in the nominal stress, as the smectic polydomain undergoes an elastic deformation. If the elastomer is stretched to an overall draw ratio lying within Region I, the material relaxes completely when the tension is released, as observed photographically by the ink-dot technique. The polydomain LCE behaves essentially as a stiff, rubber-like network within Region I.

The end of Region I signifies yielding of the polydomain, marking the onset of the P−M transition. In the force ramp tensile test, Region II is characterized by a rapid uniaxial elongation at a nearly constant value of σ_n, producing the well-known "plateau" in the stress−strain curve. In the strain ramp tensile test, the onset of Region II is characterized by a pronounced decrease in the nominal stress, which is followed by a gradual increase in σ_n as λ approaches 4.0. From the strain ramp tensile test data, a yield stress of $\sigma_y = 1.65$ MPa is

identified at $\lambda_y = 1.18$ by construction of a Considére tangent.[25] The drop in the nominal stress after yielding is more than 40% of σ_y at the chosen rate of elongation. During the strain ramp test, the sample experiences a steady increase in the nominal stress as it passes through the "plateau" region. The true stress may increase at an even higher rate due to contraction of the sample. It is interesting to note that Griffin et al. reported similar yielding behavior in a smectic elastomer having "transverse rod" mesogens in the main chain.[26]

In the strain ramp method, the yielding coincides with the onset of necking, a macroscopic mechanical instability characterized by a localized contraction of the elastomer, which initiates at some stress concentrator, often at the thinnest portion of the sample. Once necking initiates, the local draw ratio (λ_m) becomes spatially nonuniform. The value of λ_m in the thicker (non-necked) portion of the sample is always less than or equal to λ_y, while the value of λ_m in the thinner (necked) portion is always greater than or equal to λ. It is sometimes possible for more than one neck to form in the same sample if multiple stress concentrators are present. Despite widespread observations of the plateau stress phenomenon in LCE, necking instabilities have infrequently been reported.[7,26−29] It is possible that a clearly defined neck is observed only under certain conditions of temperature and strain rate. In non-cross-linked polymers, the geometry of the neck region varies with strain rate and temperature,[30] and the observed value of σ_n depends strongly upon elongation rate due to thermomechanical coupling effects.[31] Thus, it is possible that neck formation has been overlooked in previous studies of LCE because the materials were subjected to elongation under conditions different from those employed in this investigation. It is also possible that some LCEs do not exhibit necking instabilities under any conditions.

Figure 4 shows the necking transition as it appears through partially crossed polarizers in the light microscope, after stretching manually at 22 °C. Figure 4a shows the necking instability at an overall draw ratio of $\lambda = 1.18$, a few minutes after the neck first appeared. Figure 4b shows the growth of the necked portion at $\lambda = 1.54$. The highest birefringence is observed within the necked portion of the sample, indicating substantially higher molecular anisotropy in that region. The necked portion has essentially reached the monodomain state, while the remainder of the elastomer remains in the polydomain state. A thin boundary region separates the polydomain and monodomain portions of the sample, as shown in Figure 4c. Stretching the elastomer in situ revealed that the P−M transition occurs in a localized fashion near and within the boundary region. As elongation proceeds, the monodomain portion of the sample increases in length while appearing to consume polydomain material at its boundaries.

If the overall draw ratio is held constant within Region II for some time, the monodomain portion can increase in length slightly, with loss of some additional polydomain material. During this time, the value of λ_m within the polydomain regions may actually decrease to as low as 1.01, well below the value of λ_y. Thus, stress relaxation can occur in Region II by conversion of polydomain material to (necked) monodomain material. In a strain ramp at a sufficiently low rate of elongation, the same effect is expected: the value of λ_m in the non-necked, polydomain region may actually decrease once the material yields because the nominal stress drops significantly.

The end of Region II is reached once the necked region consumes all of the polydomain material. In both types of tensile tests, an increase in the nominal stress is seen at the highest elongations studied (Region III), due in part to the higher free energy cost for stretching of the fully necked monodomain elastomer. This strain hardening is reminiscent of that observed at high elongations in conventional (amorphous, noncrystallizable) elastomers due to the finite extensibility of the network chains. Strain hardening has also been observed in the cold-drawing of non-cross-linked polymers, including smectic main-chain polymers,[32] for different reasons.

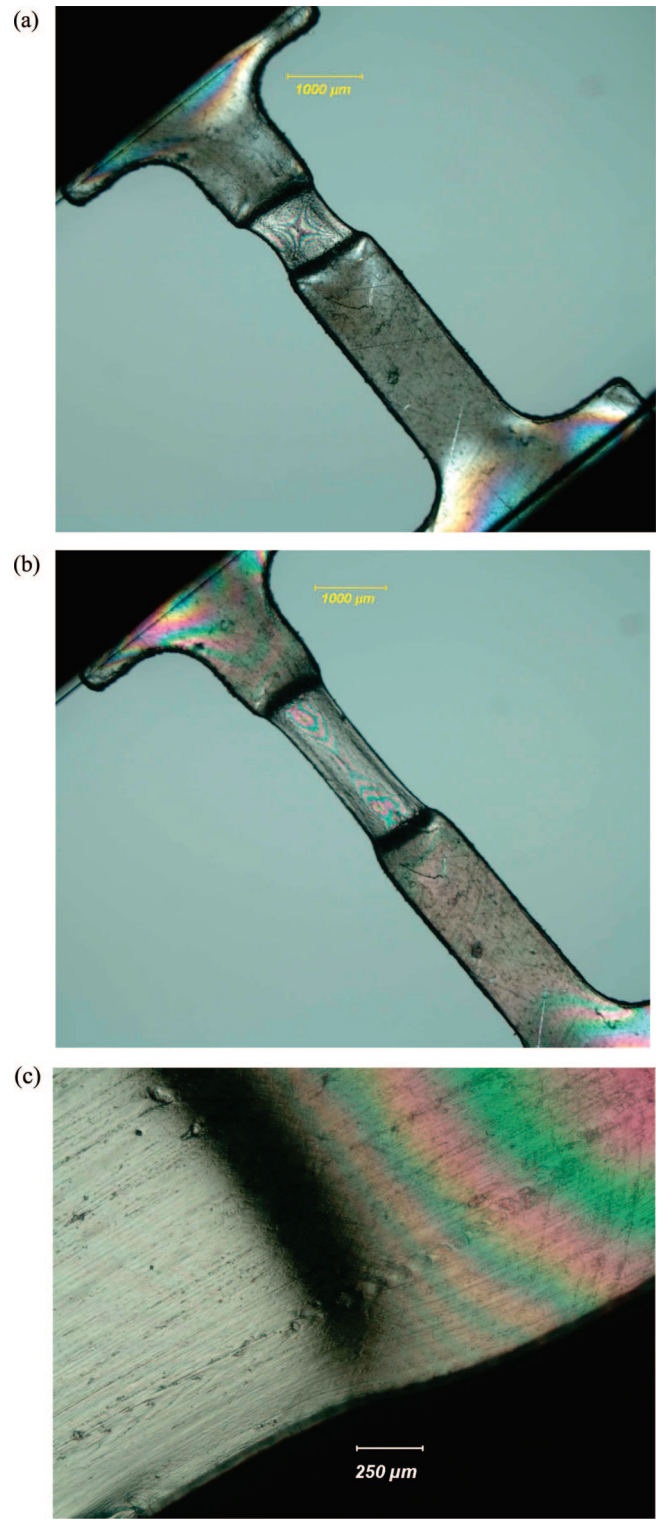

Figure 4. Polarized optical micrographs illustrating the necking instability in a smectic main-chain LCE under uniaxial extension. (a) $\lambda = 1.18$; (b) $\lambda = 1.54$; (c) close-up of boundary region separating necked material (left) from non-necked material (right).

3.3. WAXD Characterization. Changes in molecular orientation occurring during the P−M transition were characterized by wide-angle X-ray diffraction (WAXD). The sample was held under tension during WAXD using a portable clamping device.

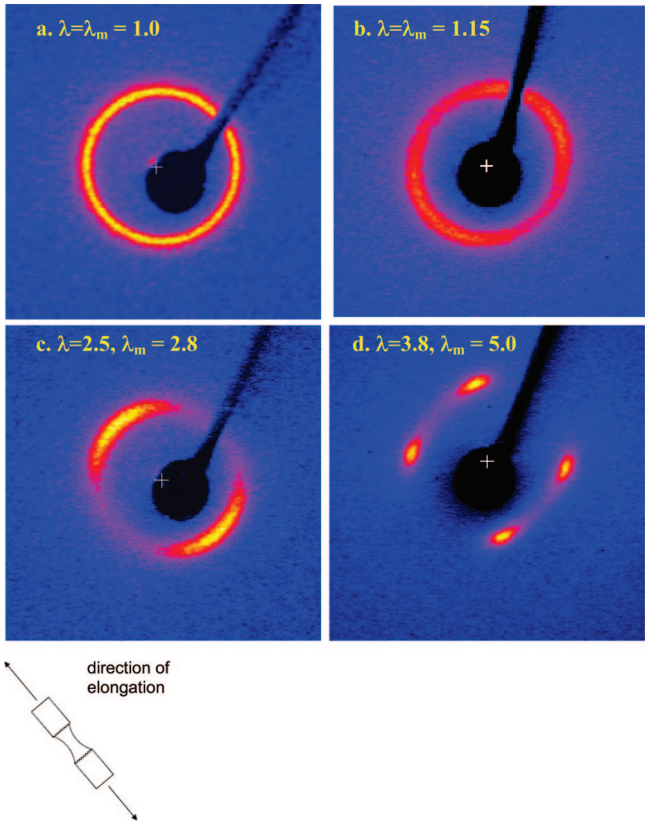

Figure 5. WAXD patterns for the elastomer at different overall draw ratios (λ). The mesoscopic draw ratio (λ_m) was determined at the point where the beam passed through the sample. The low-angle reflection is centered at $2\theta \approx 2.9°$ in the unperturbed state.

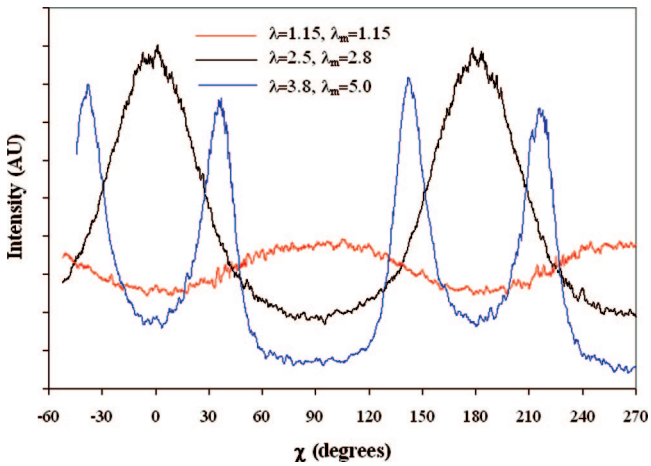

Figure 6. Diffracted intensity versus azimuthal angle for uniaxially elongated smectic main-chain LCE at different overall draw ratios (λ) at 25 °C. Data points near the beamstop are omitted for clarity.

The evolution of the smectic layer orientation was deduced from the azimuthal intensity distribution of the strong, low-angle layering reflection centered near $2\theta \approx 2.9°$. Figure 5 shows diffraction patterns obtained at overall draw ratios of $\lambda = 1.0$ (unperturbed polydomain state), $\lambda = 1.15$ (Region I), $\lambda = 2.5$ (middle of Region II), and $\lambda = 3.8$ (onset of Region III). The beam passed through the center of the necked region for the latter two patterns, and the local draw ratio λ_m is noted in each case. Figure 6 presents integrated intensity versus azimuthal angle (χ) for the diffraction patterns presented in Figure 5b−d.

The initial orientation of layer normals is random, indicated by the isotropic diffraction ring at low angle in Figure 5a, as expected. Within Region I at $\lambda = 1.15$, the equatorial enhancement of the intensity indicates rotation of smectic layer normals (and chain axes) away from z. Figure 6 illustrates that the smectic layer normals, which are assumed to be parallel to the chain axes, are preferably oriented perpendicular to z at $\lambda = 1.15$. Broad peaks in the diffracted intensity are centered near $\chi = 90°$ and $\chi = 270°$. Although the net orientational order is weak, the observed changes confirm the assertion that local director rotations play a significant role in the P−M transition. The director rotations initiate in Region I in this elastomer, before the P−M transition appears.

Previous experimental work revealed the "anomalous" or perpendicular orientation of chain axes with respect to z during elongational flow of linear, non-cross-linked smectic main-chain polymers.[2,21,32−40] However, the perpendicular orientation of the chain axes has seldom been observed in cross-linked, main-chain elastomers.[22] (One must distinguish the orientation of chain axes from the orientation of mesogenic groups, which may or may not coincide with chain axes, especially in side-chain LCE.) In some cases, both the "normal" orientation (chain axes parallel to axis of elongation) and the "anomalous" orientation (chain axes perpendicular to axis of elongation) can be observed in the same polymer under different conditions of temperature or strain rate,[22,33−35,37,38,40] but only the normal orientation is reported in most studies of main-chain elastomers. We previously observed the anomalous orientation in an elongated sample of a linear, non-cross-linked polymer (M_w = 85 kg mol^{-1}) that had the same chemical backbone as the elastomer in this study.[2]

The anomalous orientation results when anisotropically shaped, chain-folded microdomains align with the draw direction, rotating chain axes perpendicular to z (illustrated schematically in Figure 7). Within the ordered regions of smectic main-chain polymers[21] and elastomers,[3,23] chains are expected to adopt a hairpinned or folded backbone conformation. The initial deformation of the polydomain elastomer (Region I) follows a pathway that minimizes the work of deformation, which involves rotation of domains with minimal disruption to segment-level ordering within domains. The apparent Young's modulus is quite high (~9 MPa), as the chain-folded smectic microdomains serve as weak physical cross-links due to their tendency to maintain smectic ordering. Because the anomalous orientation of chain axes is slightly preferred at draw ratios less than $\lambda = 1.18$, we infer that the chain axes lie orthogonal to the long axes of the smectic domains. The chain folding in melt-crystallized and solution-crystallized semicrystalline polymers follows the same paradigm: chain axes are generally orthogonal to the largest dimensions of chain-folded lamellae. Therefore, the existence of chain-folded, lamellar domains in the smectic LCE might reasonably account for the anomalous orientation effect seen in Region I.

Following the first appearance of the neck at $\lambda = 1.18$, the elastomer enters Region II, the partially necked state. At $\lambda = 2.5$ ($\lambda_m = 2.8$), the longitudinal intensification of the low-angle reflection to form two arcs (Figures 5 and 6) indicates alignment of chain axes and smectic layer normals parallel to z. These data suggest that the yielding process involves unfolding of hairpinned chains within smectic domains to produce nearly extended elastic chains, which are oriented parallel to z, as illustrated schematically in Figure 7c. The yielding process is attributed to the transient disordering of smectic domains, as hairpins begin to unfold under high local stress. The 90° rotation in orientational order during the P−M transition is attributed to the growth of new, highly aligned smectic domains from extended chains. This assertion is supported by the large increase in local draw ratio (λ_m) observed in passing through the necking transition, which is consistent with unfolding of hairpinned coils.

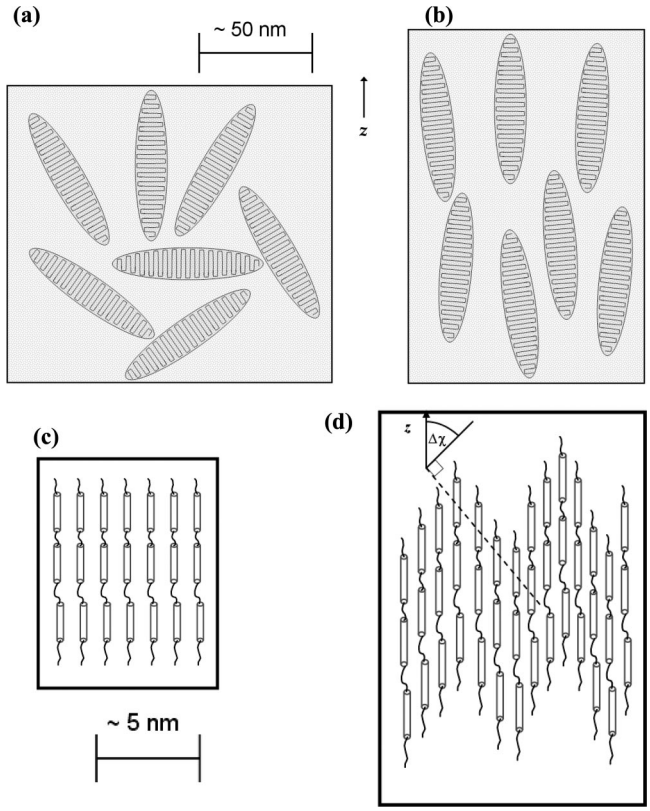

Figure 7. Evolution of molecular orientation during P−M transition in a main-chain smectic elastomer. (a) Chain-folded smectic microdomains are initially randomly oriented. Chain axes are orthogonal to the longest dimension of the domains, which are presumed to be anisotropically shaped. (b) After a small uniaxial strain (Region I), chain axes exhibit "anomalous" orientation with respect to z due to local director rotations. (c) After passing through the necking transition, few hairpinned chains remain, and chain axes favor extended conformations with preferred orientation parallel to z. (d) At high elongations, increase of the true stress affects the backbone conformation of the elastic chains, resulting in layer buckling.

Additional evidence for the formation of new smectic domains in Region II is found in the slow stress relaxation noted in the monodomain portion of the sample after removing the tension. If the necked elastomer is held under tension for several minutes, the necked condition is observed to persist essentially indefinitely without tension. The elastomer in this study remained necked in the absence of tension for at least 1 year at 22 °C, despite being above its glass transition temperature. (Note that no evidence for crystallization was detected by WAXD.) The extraordinarily slow stress relaxation in highly elongated, smectic main-chain LCE is already well-known,[7,41,42] leading to their classification as shape-memory materials.[41] These observations suggest that new smectic domains are formed after the necking transition. Once new smectic domains are formed, the elastomer is unable to relax to the (lowest energy) polydomain state without disrupting the newly formed smectic layering. The elastomer must overcome an energy barrier associated with the smectic layering to return to the polydomain state. The magnitude of this energy barrier should depend on the energy cost for disrupting smectic ordering, which should decrease with increasing temperature. Thus, it is not surprising that the elastomer returns to the non-necked, polydomain state within a few minutes upon heating to 70 °C, slightly below its clearing temperature range.

The transition from Region II to Region III occurs once the neck has propagated throughout the entire sample, reaching the clamps, such that no polydomain material remains. This fully necked, monodomain state is reached at approximately $\lambda = 3.7$, judging by the increase in stress noted in the strain ramp tensile test. At least two factors contribute to the upturn in the stress in Region III. First, as the necking transition approaches the clamps, the dogbone-shaped sample becomes thicker, producing an artificial upturn. Second, the finite extensibility of the network chains is expected to contribute to the observed upturn in the nominal stress, as in most elastomers. The fully necked sample could be elongated to $\lambda_m = 5.1$ before rupturing. The LCE retains some elastic character even in the fully necked state, as a quick relaxation to $\lambda_m \approx 4.4$ was noted after removing the tension, followed by ultraslow relaxation in the necked condition.

The WAXD data in Figures 5 and 6 reveal buckling or undulation in the smectic layers in Region III ($\lambda = 3.8$, $\lambda_m = 5.0$). The two peaks in the low-angle diffracted intensity split into four distinct maxima, indicating local rotations of the layer normals away from z. Figure 5d is similar to that expected for a globally oriented S_C elastomer, but previous studies of optical textures in the non-cross-linked polymer of the same chemical structure ruled out the S_C phase in favor of the less well-known S_{CA} phase.[2] The peak diffracted intensity was observed at $\Delta\chi = \pm 37°$, where $\Delta\chi$ is approximately equal to the angle between a smectic layer normal and z, illustrated schematically in Figure 7d, due to the low value of the Bragg angle. Under the conditions of temperature and elongation rate studied here, the buckling was first observed as Region III is approached, but it may be possible to observe buckling earlier in Region II under different conditions that favor higher true stress in the necked region. Buckling instabilities have been observed in strained S_A liquid crystals of low molar mass.[43−45] In addition, Nishikawa and Finkelmann discovered layer undulations upon straining of an S_A liquid single-crystal elastomer that was cross-linked in the globally oriented state.[46] It is interesting to note the same phenomenon occurring at high strains in a stretched polydomain LCE.

It is not yet clear whether the buckling persists indefinitely in the stretched elastomer. In a linear, non-cross-linked polymer having similar chemical structure (with methyl-substituted mesogens), the buckling instability was observed to relax slowly after elongation, eventually disappearing.[2] However, the buckling instability persists for a long time at ambient temperature in this elastomer, perhaps because the system is well below its clearing temperature. The buckling likely signifies a drastic change in backbone conformation of the elastic chains in response to high local stresses. Once the tension is removed, the chains may gradually return to a lower-energy conformation, even if their axes remain highly aligned, with the apparent loss of buckling.

4. Summary and Conclusions

The P−M transition in the smectic main-chain LCE studied was shown to occur in three stages: elastic deformation (Region I), neck propagation (Region II), and deformation of the fully necked monodomain (Region III). Under uniaxial tension, the smectic main-chain LCEs initially deform by local director rotations that favor the anomalous, or perpendicular, orientation of chain axes with respect to z. A yield stress is observed at the end of Region I, signifying the first appearance of a neck. The neck lengthens in passing through Region II. Once the neck consumes the entire sample, the elastomer has reached its globally oriented monodomain state. Layer buckling was observed in Region III, although the buckling might be observed earlier in Region II at a different temperature or strain rate. The slow stress relaxation in necked smectic main-chain LCE is attributed to the formation of new, highly elongated smectic microdomains in the necked region, which creates an energy barrier that opposes the return of the sample to the lowest energy polydomain state upon removal of the tension.

In summary, we have characterized several salient features of the P−M transition in smectic main-chain elastomers. First, the P−M transition was shown to proceed in a macroscopically inhomogeneous fashion due to a necking instability, at least under the specific conditions of temperature and elongation rate studied here. The appearance of the necking instability coincides with a dramatic drop in the nominal stress, which is noted only in the strain ramp tensile test. The observed "plateau" stress in controlled-force elongation experiments is attributed to the growth of the necked region. Further work should examine how the rate of elongation and the temperature influence the geometry of the neck and the observed value of the yield stress. A second key insight is that perpendicular or "anomalous" orientation of chain axes with respect to z occurs in Region I. This observation provides direct evidence that local director rotations precede the P−M transition in smectic main-chain LCE, whereby the long axes of anisotropically shaped domains rotate to align with z, similar to the model of nematic elastomers proposed by Fridrikh and Terentjev.[13] It is possible that local domain rotations concentrate the stress locally, and therefore initiate the pulling out of hairpins and trigger the necking instability. Finally, we have shown that layer buckling can be observed in uniaxially elongated polydomain smectic LCE, whereas previous reports have exclusively demonstrated layer buckling in LCE cross-linked in the monodomain state.

Acknowledgment. This work was supported by the U.S. National Science Foundation under grant DMR-0733658.

References and Notes

(1) Patil, H. P.; Hedden, R. C. *J. Polym. Sci., Part B: Polym. Phys.* **2007**, *45*, 3267–3276.
(2) Patil, H. P.; Liao, J.; Hedden, R. C. *Macromolecules* **2007**, *40*, 6206–6216.
(3) Ishige, R.; Osada, K.; Tagawa, H.; Niwano, H.; Tokita, M.; Watanabe, J. *Macromolecules* **2008**, *41*, 7566–7570.
(4) Adams, J. M.; Warner, M. *Phys. Rev. E* **2005**, *71*, 021708-1–021708-15.
(5) Adams, J. M.; Warner, M. *Phys. Rev. E* **2005**, *72*, 011703-1–011703-8.
(6) Beyer, P.; Terentjev, E. M.; Zentel, R. *Macromol. Rapid Commun.* **2007**, *28*, 1485–1490.
(7) Ortiz, C.; Wagner, M.; Bhargava, N.; Ober, C. K.; Kramer, E. J. *Macromolecules* **1998**, *31*, 8531–8539.
(8) Ortiz, C.; Ober, C. K.; Kramer, E. J. *Polymer* **1998**, *39*, 3713–3718.
(9) Finkelmann, H.; Kock, H. J.; Gleim, W.; Rehage, G. *Makromol. Chem., Rapid Commun.* **1984**, *5*, 287–293.
(10) Hammerschmidt, K.; Finkelmann, H. *Makromol. Chem.* **1989**, *190*, 1089–1101.
(11) Zubarev, E. R.; Talroze, R. V.; Yuranova, T. I.; Plate, N. A.; Finkelmann, H. *Macromolecules* **1998**, *31*, 3566–3570.
(12) Hotta, A.; Terentjev, E. M. *J. Phys.: Condens. Matter* **2001**, *13*, 11453–11464.
(13) Fridrikh, S. V.; Terentjev, E. M. *Phys. Rev. E* **1999**, *60*, 1847–1857.
(14) Schatzle, J.; Kaufhold, W.; Finkelmann, H. *Makromol. Chem.* **1989**, *190*, 3269–3284.
(15) Clarke, S. M.; Terentjev, E. M.; Kundler, I.; Finkelmann, H. *Macromolecules* **1998**, *31*, 4862–4872.
(16) Clarke, S. M.; Nishikawa, E.; Finkelmann, H.; Terentjev, E. M. *Macromol. Chem. Phys.* **1997**, *198*, 3485–3498.
(17) Fridrikh, S. V.; Terentjev, E. M. *Phys. Rev. Lett.* **1997**, *79*, 4661–4664.
(18) Terentjev, E. M.; Warner, M.; Verwey, G. C. *J. Phys. II* **1996**, *6*, 1049–1060.
(19) Warner, M.; Terentjev, E. M. *Prog. Polym. Sci.* **1996**, *21*, 853–891.
(20) Warner, M.; Bladon, P.; Terentjev, E. M. *J. Phys. II* **1994**, *4*, 93–102.
(21) Tokita, M.; Osada, K.; Watanabe, J. *Liq. Cryst.* **1997**, *23*, 453–456.
(22) Zentel, R.; Schmidt, G. F.; Meyer, J.; Benalia, M. *Liq. Cryst.* **1987**, *2*, 651–664.
(23) Adams, J. M.; Warner, M. *Eur. Phys. J. E* **2005**, *16*, 97–107.
(24) Donnio, B.; Wermter, H.; Finkelmann, H. *Macromolecules* **2000**, *33*, 7724–7729.
(25) Ward, I. M.; Sweeney, J. *An Introduction to the Mechanical Properties of Solid Polymers*, 2nd ed.; Wiley: Chichester, West Sussex, 2004; Chapter 11, pp 245−249.
(26) Ren, W.; McMullan, P. J.; Guo, H.; Kumar, S.; Griffin, A. C. *Macromol. Chem. Phys.* **2008**, *209*, 272–278.
(27) Warner, M.; Terentjev, E. M. *Liquid Crystal Elastomers*; Clarendon Press: Oxford, 2003.
(28) Hedden, R. C.; Tachibana, H.; Duncan, T. M.; Cohen, C. *Macromolecules* **2001**, *34*, 5540–5546.
(29) Hedden, R. C.; Saxena, H.; Cohen, C. *Macromolecules* **2000**, *33*, 8676–8684.
(30) Allison, S. W.; Andrews, R. D. *J. Appl. Phys.* **1967**, *38*, 4164–4168.
(31) Boyce, M. C.; Montagut, E. L.; Argon, A. S. *Polym. Eng. Sci.* **1992**, *32*, 1073–1085.
(32) Fernandez-Blazquez, J. P.; Bello, A.; Cerrada, M. L.; Perez, E. *Macromolecules* **2008**, *41*, 421–428.
(33) Bello, P.; Bello, A.; Lorenzo, V. *Polymer* **2001**, *42*, 4449–4452.
(34) Bello, P.; Bello, A.; Riande, E.; Heaton, N. J. *Macromolecules* **2001**, *34*, 181–186.
(35) Fernandez-Blazquez, J. P.; Bello, A.; Perez, E. *Macromolecules* **2007**, *40*, 703–709.
(36) Leland, M.; Wu, Z. Q.; Chhajer, M.; Ho, R. M.; Cheng, S. Z. D.; Keller, A.; Kricheldorf, H. R. *Macromolecules* **1997**, *30*, 5249–5254.
(37) Martinez-Gomez, A.; Perena, J. M.; Lorenzo, V.; Bello, A.; Perez, E. *Macromolecules* **2003**, *36*, 5798–5803.
(38) Osada, K.; Koike, M.; Tagawa, H.; Hunaoka, S.; Tokita, M.; Watanabe, J. *Macromolecules* **2005**, *38*, 7337–7342.
(39) Tokita, M.; Osada, K.; Kawauchi, S.; Watanabe, J. *Polym. J.* **1998**, *30*, 687–690.
(40) Tokita, M.; Tokunaga, K.; Funaoka, S.; Osada, K.; Watanabe, J. *Macromolecules* **2004**, *37*, 2527–2531.
(41) Rousseau, I. A.; Mather, P. T. *J. Am. Chem. Soc.* **2003**, 15300–15301.
(42) Ren, W.; McMullan, P. J.; Griffin, A. C. *Macromol. Chem. Phys.* **2008**, *209*, 1896–1899.
(43) de Gennes, P. G.; Prost, J. *The Physics of Liquid Crystals*; Clarendon Press: Oxford, 1993.
(44) Delaye, M.; Ribotta, R.; Durand, G. *Phys. Lett. A* **1973**, *A44*, 139–140.
(45) Clark, N. A.; Meyer, R. B. *Appl. Phys. Lett.* **1973**, *22*, 493–494.
(46) Nishikawa, E.; Finkelmann, H. *Macromol. Chem. Phys.* **1999**, *200*, 312–322.

MA9001325